Tuning the Structure of Nickelates to Achieve Two-Dimensional Electron Conduction

Divine P. Kumah, Ankit S. Disa, Joseph H. Ngai, Hanghui Chen, Andrei Malashevich, James W. Reiner, Sohrab Ismail-Beigi, Frederick J. Walker, and Charles H. Ahn**

Rare-earth perovskite nickelates (ReNiO$_3$) display complex electronic and magnetic behavior that arises from a strong interplay between atomic-scale structure and electronic correlations on the Ni sites.[1,2] Motivated by recent predictions that an electronic structure mimicking that of the high-temperature cuprate superconductors can be achieved in nickelates,[3,4] intensive theoretical and experimental research efforts have focused on controlling the energetic ordering of Ni d orbitals[5–8] and 2D conduction in nickelate heterostructures. This work has led to the realization of nickelate thin film and multilayered structures that exhibit interesting magnetic and electronic transitions, including metallic conduction in superlattices.[6,9–11] A consequence of this focus has been the discovery of an intriguing thickness-dependent metal-insulator (MI) transition in thin nickelate films reminiscent of electronic and magnetic "dead layer" effects in other correlated complex oxide systems, such as the rare-earth vanadates,[12] ruthenates[13] and manganites[14] whose properties are governed by the transition metal-oxygen bond properties. To elucidate the microscopic basis for this phenomenon, we use a combination of synchrotron X-ray structural characterization, first principles density functional theory (DFT), and transport measurements to quantify the atomic-scale distortions in nickelate thin films. We show that the thickness-dependent MI transition in the nickelates is associated with atomic-scale structural distortions that influence the Ni-O-Ni bond properties as a function of film thickness. Based on this observation, we show that by capping an insulating 3 uc $LaNiO_3$ (LNO) film with the wide band gap insulator $LaAlO_3$ (LAO), metallic behavior is induced in the 2D nickelate layer due to suppression of the surface distortions (see **Figure 1**).

The strong coupling of the magnetic and electronic properties of the rare-earth nickelates to their atomic-scale structure is known to occur due to the sensitive dependence of the Ni *3d*-O *2p* valence orbital hybridization on the geometry of the Ni-O bonding. Specific models that have been proposed to explain the MI transition observed in this system based on modifications of Ni-O bond properties and corresponding changes in the carrier itinerancy involve charge ordering,[15] orbital ordering,[4,7,16] Mott behavior,[17] and electronic bandwidth control in the charge-transfer conduction framework.[18] In contrast to the other ReNiO$_3$, which undergo temperature-dependent MI transitions, LNO is a paramagnetic metal at all temperatures due to the large ionic radius of La that suppresses the Ni-O bond distortions.

Experimentally, various researchers have found that thin LNO films undergo a MI transition as a function of thickness when the thickness is less than a critical value of 5 uc[9,10] in thin films and 3 uc for superlattices of LNO.[6,16] We find similar results for LNO grown using molecular beam epitaxy on LAO, an insulating substrate, with a critical thickness of 5 uc for vacuum-terminated films and 3 uc for LNO/LAO superlattices. The resistivity versus temperature behavior (Figure 1a) exhibits insulating behavior in uncapped films for film thicknesses of 4 uc; for 5 uc and thicker films, we observe metallic behavior (Figure 1b). The dependence of the magnetic and electronic phases of the bulk nickelates on the atomic-scale structural properties of the Ni-O bond properties suggests a similar basis for the thickness-dependent MI transition. Proposals to explain the observed MI transition in thin films and the reduced critical thickness for conductivity in superlattices[6,7,19] include interfacial constraints on octahedral connectivity,[20,21] disorder-driven localization,[9] strain,[16,22] and inter-layer percolation.[23] However, a systematic study of the structural evolution as a function of film thickness to elucidate the correlation between structure and the thickness-dependent changes in conductivity has not been reported.

To determine the atomic-scale structure of the films with thicknesses ranging from 4 uc to 7 uc, we perform synchrotron x-ray crystal truncation rod (CTR)[24,25] diffraction measurements at the Advanced Photon Source. Layer-resolved structural details of the LNO films with thicknesses ranging from 4 uc to 7 uc, including information about the Ni-O-Ni bond angles, are determined by measuring multiple CTRs for each thickness. The CTRs are converted to real space structures using the coherent Bragg rod analysis (COBRA) technique, which is a direct phasing method to analyze the CTRs that enables convergence on the real space structure without a priori knowledge of the deviations from the bulk of the film and interfacial structure.[26] The result is a three-dimensional electron density map (EDM) of the atomic structure.

An important structural feature we observe is a previously reported lattice polarization that develops in the surface layers of the films.[5] To determine the relation between the thickness-dependent MI transition and this surface distortion, we

Dr. D. P. Kumah, A. S. Disa, Dr. J. H. Ngai, Dr. H. Chen, Dr. A. Malashevich, Dr. J. W. Reiner, Dr. S. Ismail-Beigi, Dr. F. J. Walker, Prof. C. H. Ahn
Center for Research on Interface Structures and Phenomena
Department of Applied Physics
Yale University
New Haven, Connecticut, 06520, USA
E-mail: divine.kumah@yale.edu; Charles.ahn@yale.edu
Prof. C. H. Ahn
Department of Mechanical Engineering and Materials Science
Yale University
New Haven, Connecticut, 06520, USA

DOI: 10.1002/adma.201304256

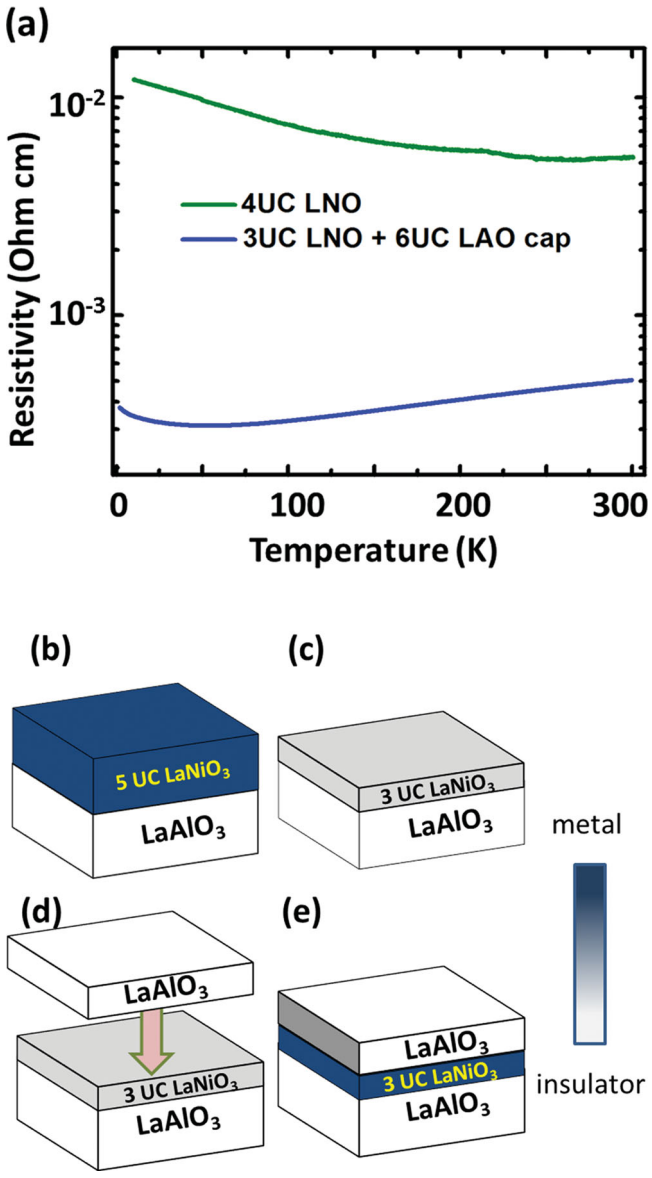

Figure 1. Manipulating the metal-insulator transition in $LaNiO_3$. (a) Resistivity versus temperature for uncapped 4 unit cell (uc) thick $LaNiO_3$ (LNO) films (green) and a 3 uc LNO film capped with 6 uc $LaAlO_3$ (LAO) (blue) grown epitaxially on (001) LAO. Schematics illustrating: (b) metallic uncapped 5 uc LNO, (c) insulating uncapped 3 uc LNO, (d) addition of an insulating 6 uc LAO capping layer, and (e) recovery of metallic transport for 3 uc LNO capped with insulating LAO. The color scale on the right represents the conductivity.

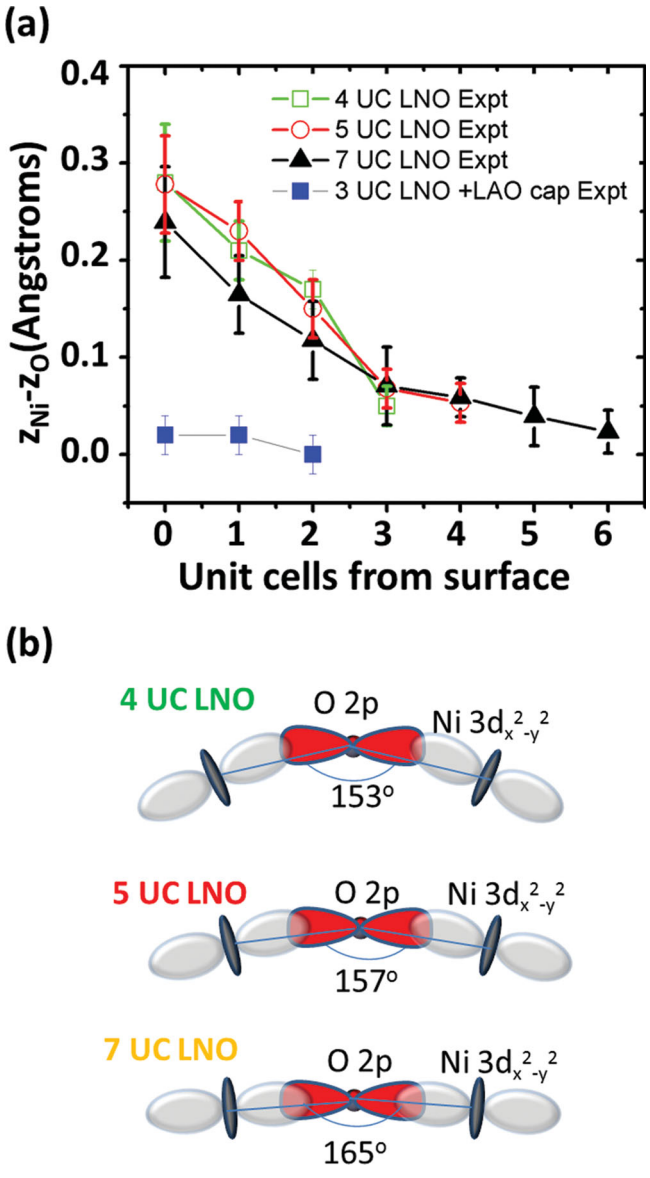

Figure 2. Structural origin of the thickness-dependent metal insulator transition. (a) Layer-resolved comparison of measured results for Ni-O vertical polar displacements, Z_{Ni}-Z_o, for uncapped 4, 5, and 7 unit cell thick $LaNiO_3$ films. The measured displacements for a 3 unit cell $LaNiO_3$ film capped with 6 unit cells of $LaAlO_3$ are shown (blue solid squares) for comparison. (b) Schematic of the measured average in-plane Ni-O-Ni bond angle for 4, 5, and 7 unit cell thick uncapped LNO films. Bond angles are exaggerated for clarity and include contributions from the polar distortions in (a) and octahedral tilts and rotations. The reduction in the Ni 3*d*-O 2*p* orbital overlap with decreasing bond angle leads to increased resistivity.

compare the measured layer-resolved polarization of LNO films with thicknesses ranging from 4 uc to 7 uc in **Figure 2**a. We find that this surface polar distortion is independent of the film thickness and is characterized by the relative displacement of the oxygen and cation z positions within both the NiO_2 and LaO (001) planes of the perovskite structure. The largest relative displacement, z_{Ni}-z_O, is at the surface, with a magnitude of ~0.3 Å, which decays to nearly zero after 3 uc towards the LNO-LAO interface (Figure 2a), resulting in a net positive polarization of the LNO films. The existence and direction of the polarization in these films can be attributed to the non-zero charge of the alternating $(LaO)^+$ and $(NiO_2)^-$ layers in the [001] direction and the termination with a negatively charged $(NiO_2)^-$ layer, resulting in a counter-dipole.[25,27] The decay of the polarization within 3 uc is observed for all thicknesses of uncapped LNO films and is consistent with electrostatic screening of the charged surface by a high density of mobile carriers in a polarizable ionic lattice. DFT-LDA calculations of the physical

structure agree quantitatively with the observed polarization magnitude, their decay, and thickness dependence.[5,28]

To more precisely quantify the effects of the polar displacements on the Ni-O bond properties, we fit[29] the measured data with a kinematic model of X-ray diffraction with a c(2 × 2) unit cell using the atomic coordinates extracted from the EDMs. The fitted structures for the films have $GdFeO_3$-like octahedral rotations with an $a^-a^-c^-$ rotation pattern in Glazer notation (i.e., along each axis, the octahedral rotations are out of phase). This rotational pattern is consistent with previous x-ray[20,22] and electron diffraction studies[30] of compressively strained LNO films and superlattices. From the best-fit structures for the 4, 5, and 7 uc thick films, we determine their respective layer-resolved Ni-O bond parameters, finding a systematic decrease in the average in-plane Ni-O-Ni angles with film thickness (Figure 2b). In contrast to structural studies on similar systems,[21,30] which lack atomic-layer resolution of the surface layers, we find that the polar distortions couple to octahedral rotations.[31]

Both the polar and octahedral distortions are expected to strongly influence electronic transport by modifying the overlap of Ni *3d*–O *2p* orbitals. This overlap is parameterized by the in-plane Ni-O-Ni bond angle θ and Ni-O bond length d; θ and d are both modified by the two distortion modes. We estimate the changes in the bond overlap using a canonical tight binding approach. Given θ and d in the x-y plane, the transfer integral t_{pd} between adjacent Ni *3d* and O *2p* orbitals is given by[18,32]

$$t_{pd} = K\frac{\cos(\varphi)}{d^{3.5}}, \quad (1)$$

where $\varphi = (180\text{-}\theta)/2$ is the effective NiO_6 octahedral tilt angle, and the pre-factor K is determined from the *p-d* orbital covalent hopping integral to be 13.7 eVÅ$^{3.5}$.[32] Larger values of t_{pd} imply a greater tendency towards metallic behavior. The bond overlap is approximately constant for each NiO_2 layer across films, but the average value shows a systematic dependence on total film thickness. The average values of t_{pd} for the 4, 5, and 7 uc films are 1.28, 1.34 and 1.41 eV, respectively. For reference, we compare these average values for our films with metallic bulk LNO[33] ($t_{pd,bulk}$ = 1.36 eV) and bulk $SmNiO_3$[34] ($t_{pd,SmNiO3}$ = 1.28 eV), which is insulating at room temperature. Based on these findings, one thus expects to find metallic behaviour for the 5 and 7 uc films, and insulating behavior for the 4 uc film, in agreement with experimental findings. The critical t_{pd} value is consistent with the energy scale of the charge transfer energy in bulk nickelates.[33]

As discussed above, the electronic bandwidth controls the MI transition. In the simplest models, where charge and/or orbital ordering opens a gap, widening of the bandwidth leads to melting of the insulating charge-ordered ground state.[33] For insulating behavior that involves charge transfer, reducing the bandwidth of the Ni e_g states reduces their overlap with the oxygen valence bands. Here too, a smaller bandwidth favors insulating behavior, where a charge-transfer gap opens between Ni e_g and O *p* valence bands below a critical t_{pd} value.[2,35]

These results reveal the quantitative structure-property relationship between polar, octahedral distortions and conductivity that drives the thickness-dependent MI transition in nickelate films. The coupling of the polar distortion to conductivity may thus play a critical role in the tuning of the MI transition using an external electrostatic gate.[36] Intrinsic thickness-dependent electronic and magnetic transitions are known to occur in other transition metal perovskite oxide systems including $SrRuO_3$,[13] $ReVO_3$,[12] and $LaAlO_3/SrTiO_3$,[25,27] which possess similar features: strong octahedral rotations and polar surfaces or interfaces. A plausible driving force of the phase transitions in these systems may be a strong coupling of polar surface/interface relaxations, which are driven by a minimization of the electrostatic free energy, to changes in transition metal-oxygen hybridization through octahedral rotations.[31]

We now show that capping the *insulating* LNO films with another *insulating* material, LAO, can induce 2D metallicity. One clear prediction of our above findings that correlate the surface distortion and conductivity is that the suppression of these distortions should lead to the recovery of a metallic ground state. To test this prediction experimentally, we begin with an insulating 3 uc LNO film and encapsulate the terminal $(NiO_2)^-$ layer with insulating LAO layers (Figure 1c-1e): the LAO serves both to encase the LNO layers and also to suppress the polar field from the charged top layer. Structural analysis of fundamental and superstructure CTRs (**Figure 3**a and Figure 3b) reveals an absence of polar distortions in the embedded LNO layers (Figure 2a) and bulklike Ni-O-Ni bond angles (162° for the LAO capped LNO, compared with 153° for the 4 uc-thick film), in good agreement with recent measurements on nickelate superlattices.[20,21] These results show directly that a bulklike structure can be recovered by structural coupling at the LNO/LAO interface which suppresses the polar distortion and octahedral rotations.

The key result of this paper is shown in Figure 1a, where we show temperature-dependent transport data for the LAO-capped 3 uc LNO sample compared with an uncapped 4 uc film. At room temperature, the resistivity of the capped sample is an order of magnitude lower than that of the 4 uc film, indicative of increased orbital overlap resulting from the absence of polar distortions. We observe metallic behavior for the capped samples as a function of temperature, in contrast to insulating behavior for the 4 uc film, demonstrating the recovery of a metallic state. We note that the metallic behavior of the capped sample rules out inter-layer percolative effects as the cause of enhanced metallicity in nickelate superlattices.[23] We also note that the absolute resistivity of the metallic capped sample is larger than the metallic uncapped 5 uc sample. The conductivity is a convolution of the bandwidth, which is controlled by the bond overlap parameters, and the charge carrier mean free path. The difference may be attributed to a decrease in the carrier mean free path in the capped sample.

The metallic conductivity of the capped sample is different in character from bulk LNO due to the 2D confinement of the carriers. Below 25 K, we observe a transition to weakly insulating transport behavior, characteristic of a 2D metal with finite disorder.[37] **Figure 4**a shows the sheet conductance for the bilayer sample and an $[(LNO)_3\text{-}(LAO)_5]$ x 20 superlattice as a function of ln(T) below 25 K. Both structures exhibit a linear dependence with slopes of $pe^2/\pi h$ and $p = 2$, where the inelastic mean free path, $l_{in,}$ scales as $T^{-p/2}$.[38] We also perform magnetoresistance (MR) measurements with a magnetic field oriented perpendicular to the film surface (Figure 4b) which show a

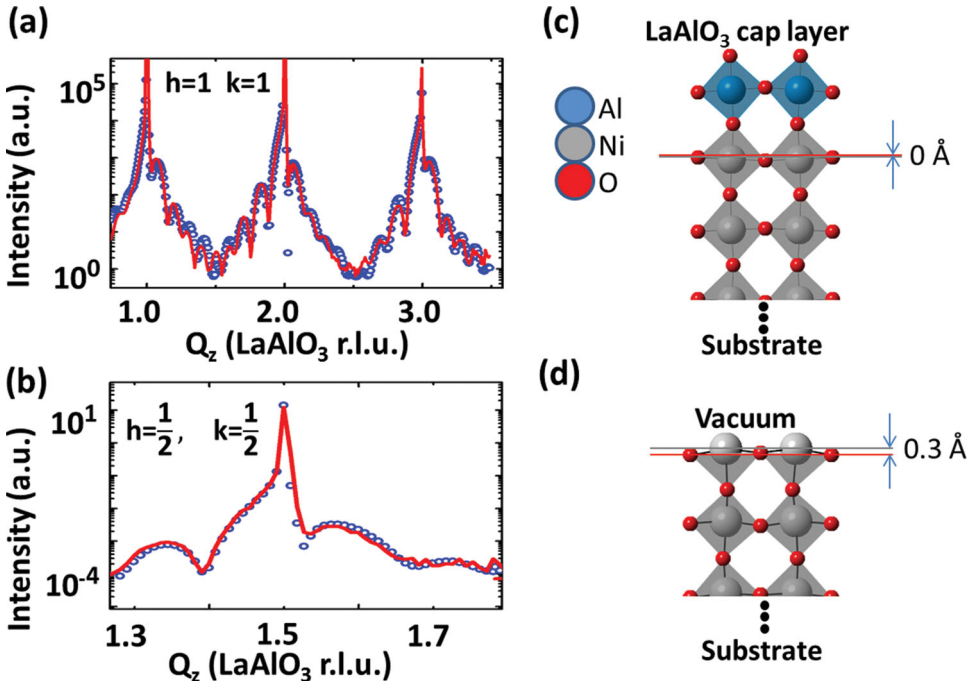

Figure 3. Recovery of a bulk-like structure. (a) Experimental fundamental [1,1,L] crystal truncation rod data (blue circles) and fits for an $LaNiO_3$ film capped with 6 uc of $LaAlO_3$. Clear finite thickness oscillations are observed in addition to the film Bragg peaks. (b) Measured [0.5 0.5 1,5] superstructure reflections (blue circles) and associated fits (red line). (c) Atomic structure positions obtained from converged fits in (a) and (b), showing the top two LNO layers in a capped 3 unit cell sample. (d) Model structure of the top two layers of an uncapped 4 unit cell LNO film, with polar vertical Ni-O displacements that are absent in the capped structure shown in (c). The horizontal red and gray lines in (c) and (d) indicate the vertical coordinates of the O and Ni sublattices in the top NiO_2 planes, respectively.

negative MR characteristic of 2D weak localization (WL).[9,10,39] As previously observed,[9] the MR is found to be isotropic with the field direction, which is unexpected for weakly localized 2D metals, but has been observed in 2D metallic systems with spin fluctuations.[6,9,40,41] If the magnetic scattering from spin fluctuations enhances the negative MR,[40] then we obtain a lower bound on l_{in} that varies from ~1.5 nm at 25 K to ~10 nm at 3 K (Figure 4c).

In summary, we determine structural parameters of nickelate heterostructures that are correlated with the MI transition in LNO films and superlattices using synchrotron scattering and first-principles theory. We identify polar distortions and octahedral rotations as the structural parameters controlling the MI transition through carrier band narrowing, in addition to a surface orbital polarization.[5] The presence of a free surface enhances these structural distortions. By encapsulating the surface with fully insulating spacer layers, we eliminate the polar distortions and restore bulk-like octahedral rotations, which in turn leads to a recovery of metallic conductivity in 2D nickelate systems. These results quantitatively relate the bonding geometry with band parameters that are important inputs to theoretical models of electronic behavior. The observed structural

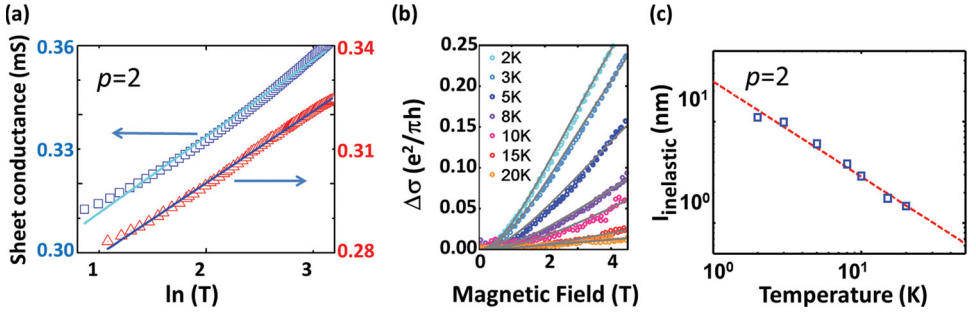

Figure 4. 2D metallicity in $LaNiO_3$. (a) Sheet conductance as a function of ln(T) for a capped 3 uc LNO film (blue squares) and an $[(LaNiO_3)_3$-$(LaAlO_3)_5]$ x 20 superlattice (red triangles) in the weakly insulating range T< 25 K. The slope of the linear fit, indicated by the solid lines, is given by pe^2/π., The superlattice resistivity is normalized to the total thickness of the $LaNiO_3$ layers. (b) Magnetoconductance $[\Delta\sigma(H) = \sigma(H)\text{-}\sigma(H = 0)]$ for increasing temperature in the range 2 K – 20 K for an $[(LaNiO_3)_3$-$(LaAlO_3)_5]$ x 20 superlattice. The solid lines represent best fits to the data from Eq. (S1) of the Supplementary material. The magnetic field is parallel to the surface normal. (c) Inelastic scattering length plotted as a function of temperature for an $[(LaNiO_3)_3$-$(LaAlO_3)_5]$x 20 superlattice, with a linear fit to the data. Both axes are on a logarithmic scale. The values for $l_{inelastic}$ are obtained from the fits from (b).

distortions have recently been shown to play a critical role in breaking the orbital degeneracy in this system.[5] The ability to tune these parameters, as demonstrated here, will lead to a deeper understanding of electronic behavior in broad classes of materials, including layered 2D electronic systems, such as chalcogenides[42] and other related complex oxide systems, such as iridates and vanadates.

Experimental Section

Capped and uncapped LNO thin films are grown on LAO (100) substrates using oxygen-plasma assisted molecular beam epitaxy, producing an in-plane compressive lattice strain of ~1% compared with bulk LNO. A growth rate of 1 uc/minute is used at a substrate temperature of 590 °C. During growth, reflection high energy electron diffraction is used to monitor the crystallinity of the sample surface and film thickness. The samples are cooled in situ in an oxygen plasma, followed by an *ex situ* anneal in flowing oxygen at 600 °C for 6 hours to ensure oxygen stoichiometry. Atomic force microscope images reveal smooth surfaces. Typical films have ~1 Å root-mean-square roughness and well defined steps with unit cell height and ~180 nm width. The Ni^{3+} oxidation state of the films and superlattices is confirmed by x-ray absorption (XAS) measurements at the Ni *L* edge carried out at the U4B beamline at the National Synchrotron Light Source (NSLS).

Room temperature synchrotron diffraction measurements are performed at the XOR 33ID beamline at the Advanced Photon Source and the X22 beamline at NSLS. During the measurements, the samples are mounted in an evacuated Be-dome chamber pumped to 10^{-5} Torr to avoid X-ray beam-induced sample damage. Surface diffraction intensities are measured along the LAO pseudocubic crystal truncation rods using either an X-ray energy of 16.0 keV ($\lambda = 0.77$ Å) or 8.2 keV. The diffracted intensity along the crystal truncation rods[24] of the substrate is measured using a solid state area detector at 300 K for each sample along crystal truncation rods for integer Miller index h,k values, where $-3 < h$ and $k < 3$.

For electrical transport, DC electrical resistivity and Hall effect measurements are carried out using Van der Pauw and four point configurations with sputtered Au contacts in a shielded cryostat over a temperature range of 1.5–300 K. Magnetic fields up to 5 T are used to obtain magneto-transport data.

For theoretical calculations, density functional theory (DFT) is used to calculate the ground state structure of thin films of (001) LNO on LAO substrates and (001) LNO/LAO superlattices, starting with initially non-polar structures. In the thin film calculations, periodic copies along the *z* direction are separated by a large vacuum gap of ~20 Å to simulate isolated surfaces. In all calculations, the in-plane (*x* and *y*) directions of the simulation cells are subject to periodic boundary conditions and fixed to the theoretical lattice constant of LAO at 3.71 Angstroms (2% smaller than the experimental value). Further technical details of the simulations are found in the Supplementary material.[28]

Supporting Information

Supporting Information is available from the Wiley Online Library or from the author.

Acknowledgements

Work at Yale is supported by grant W911NF-10–1–0206 from the Army Research Office, with funding from the DARPA OLE Program, and NSF DMR-1119826 (CRISP). Use of the Advanced Photon Source is supported by the U.S. Department of Energy, Office of Science, Office of Basic Energy Sciences, under Contract No. DE-AC02–06CH11357. Use of the National Synchrotron Light Source, Brookhaven National Laboratory, is supported by the U.S. Department of Energy, Office of Science, Office of Basic Energy Sciences, under Contract No. DE-AC02–98CH10886. Partial personnel and facilities support is provided by NSF grant CNS 08–21132 and by the facilities and staff of the Yale University Faculty of Arts and Sciences High Performance Computing Center.

Received: August 23, 2013
Revised: January 9, 2014
Published online: February 3, 2014

[1] G. Catalan, *Phase Transitions* **2008**, *81*, 729.
[2] M. L. Medarde, *J. Phys.: Condensed Matter* **1997**, *9*, 1679.
[3] P. Hansmann, A. Toschi, X. Yang, O. K. Andersen, K. Held, *Phys. Rev. B* **2010**, *82*, 235123.
[4] J. Chaloupka, G. Khaliullin, *Phys. Rev. Lett.* **2008**, *100*, 016404.
[5] H. Chen, D. P. Kumah, A. S. Disa, F. J. Walker, C. H. Ahn, S. Ismail-Beigi, *Phys. Rev. Lett.* **2013**, *110*, 186402.
[6] A. V. Boris, Y. Matiks, E. Benckiser, A. Frano, P. Popovich, V. Hinkov, P. Wochner, M. Castro-Colin, E. Detemple, V. K. Malik, C. Bernhard, T. Prokscha, A. Suter, Z. Salman, E. Morenzoni, G. Cristiani, H. U. Habermeier, B. Keimer, *Science* **2011**, *332*, 937.
[7] E. Benckiser, M. W. Haverkort, S. Bruck, E. Goering, S. Macke, A. Frano, X. P. Yang, O. K. Andersen, G. Cristiani, H. U. Habermeier, A. V. Boris, I. Zegkinoglou, P. Wochner, H. J. Kim, V. Hinkov, B. Keimer, *Nat. Mater.* **2011**, *10*, 189.
[8] M. J. Han, M. van Veenendaal, *Phys. Rev. B* **2011**, *84*, 125137.
[9] R. Scherwitzl, S. Gariglio, M. Gabay, P. Zubko, M. Gibert, J. M. Triscone, *Phys. Rev. Lett.* **2011**, *106*, 246403.
[10] J. Son, P. Moetakef, J. M. LeBeau, D. Ouellette, L. Balents, S. J. Allen, S. Stemmer, *Appl. Phys. Lett.* **2010**, *96*, 062114.
[11] E. Sakai, M. Tamamitsu, K. Yoshimatsu, S. Okamoto, K. Horiba, M. Oshima, H. Kumigashira, *Phys. Rev. B* **2013**, *87*, 075132.
[12] P. Horsch, A. M. Oleś, L. F. Feiner, G. Khaliullin, *Phys. Rev. Lett.* **2008**, *100*, 167205.
[13] J. M. Rondinelli, N. M. Caffrey, S. Sanvito, N. A. Spaldin, *Phys. Rev. B* **2008**, *78*, 155107.
[14] J. Z. Sun, D. W. Abraham, R. A. Rao, C. B. Eom, *Appl. Phys. Lett.* **1999**, *74*, 3017.
[15] a) J. Lorenzo, J. Hodeau, L. Paolasini, S. Lefloch, J. Alonso, G. Demazeau, *Phys. Rev. B* **2005**, *71*, 045128; b) V. Scagnoli, U. Staub, M. Janousch, A. Mulders, M. Shi, G. Meijer, S. Rosenkranz, S. Wilkins, L. Paolasini, J. Karpinski, S. Kazakov, S. Lovesey, *Phys. Rev. B* **2005**, *72*, 155111; c) U. Staub, G. I. Meijer, F. Fauth, R. Allenspach, J. G. Bednorz, J. Karpinski, S. M. Kazakov, L. Paolasini, F. d'Acapito, *Phys. Rev. Lett.* **2002**, *88*, 126402; d) J. A. Alonso, M. J. Martinez-Lope, M. T. Casais, J. L. Garcia-Munoz, M. T. Fernandez-Diaz, *Phys. Rev. B* **2000**, *61*, 1756; e) I. I. Mazin, D. I. Khomskii, R. Lengsdorf, J. A. Alonso, W. G. Marshall, R. A. Ibberson, A. Podlesnyak, M. J. Martinez-Lope, M. M. Abd-Elmeguid, *Phys. Rev. Lett.* **2007**, *98*, 176406; f) S. Lee, R. Chen, L. Balents, *Phys. Rev. Lett.* **2011**, *106*, 016405.
[16] J. Chakhalian, J. Rondinelli, J. Liu, B. Gray, M. Kareev, E. Moon, N. Prasai, J. Cohn, M. Varela, I. Tung, M. Bedzyk, S. Altendorf, F. Strigari, B. Dabrowski, L. Tjeng, P. Ryan, J. Freeland, *Phys. Rev. Lett.* **2011**, *107*, 116805.
[17] a) H. Park, A. Millis, C. Marianetti, *Phys. Rev. Lett.* **2012**, *109*, 156402; b) M. K. Stewart, J. Liu, M. Kareev, J. Chakhalian, D. N. Basov, *Phys. Rev. Lett.* **2011**, *107*, 176401.
[18] J. Torrance, P. Lacorre, A. Nazzal, E. Ansaldo, C. Niedermayer, *Phys. Rev. B* **1992**, *45*, 8209.
[19] A. Blanca-Romero, R. Pentcheva, *Phys. Rev. B* **2011**, *84*, 195450.
[20] S. J. May, C. R. Smith, J. W. Kim, E. Karapetrova, A. Bhattacharya, P. J. Ryan, *Phys. Rev. B* **2011**, *83*, 153411.

[21] J. Hwang, J. Son, J. Y. Zhang, A. Janotti, C. G. Van de Walle, S. Stemmer, *Phys. Rev. B* **2013**, *87*, 060101.
[22] S. J. May, J. W. Kim, J. M. Rondinelli, E. Karapetrova, N. A. Spaldin, A. Bhattacharya, P. J. Ryan, *Phys. Rev. B* **2010**, *82*, 014110.
[23] J. Son, J. M. LeBeau, S. J. Allen, S. Stemmer, *Appl. Phys. Lett.* **2010**, *97*, 202109.
[24] I. K. Robinson, D. J. Tweet, *Rep. Prog. Phys.* **1992**, *55*, 599.
[25] S. A. Pauli, S. J. Leake, B. Delley, M. Bjorck, C. W. Schneider, C. M. Schleputz, D. Martoccia, S. Paetel, J. Mannhart, P. R. Willmott, *Phys. Rev. Lett.* **2011**, *106*, 036101.
[26] Y. Yacoby, M. Sowwan, E. Stern, J. Cross, D. Brewe, R. Pindak, J. Pitney, E. M. Dufresne, R. Clarke, *Nat. Mater.* **2002**, *1*, 99.
[27] R. Pentcheva, W. E. Pickett, *Phys. Rev. Lett.* **2009**, *102*, 107602.
[28] Suplementary Materials.
[29] M. Bjorck, G. Andersson, *J. Appl. Cryst.* **2007**, *40*, 1174.
[30] J. Hwang, J. Y. Zhang, J. Son, S. Stemmer, *Appl. Phys. Lett.* **2012**, *100*, 191909.
[31] E. Bousquet, M. Dawber, N. Stucki, C. Lichtensteiger, P. Hermet, S. Gariglio, J. M. Triscone, P. Ghosez, *Nature* **2008**, *452*, 732.
[32] W. Harrison, *The Electronic Structure and Properties of Solids*, Freeman, San Francisco **1980**.
[33] C. Cui, T. A. Tyson, *Phys. Rev. B* **2004**, *70*, 094409.
[34] J. Rodríguez-Carvajal, S. Rosenkranz, M. Medarde, P. Lacorre, M. T. Fernandez-Díaz, F. Fauth, V. Trounov, *Phys. Rev. B* **1998**, *57*, 456.
[35] S. R. Barman, A. Chainani, D. D. Sarma, *Phys. Rev. B* **1994**, *49*, 8475.
[36] R. Scherwitzl, P. Zubko, C. Lichtensteiger, J. M. Triscone, *Appl. Phys. Lett.* **2009**, *95*, 222114.
[37] a)P. A. Lee, T. V. Ramakrishnan, *Rev. Mod. Phys.* **1985**, *57*, 287; b)B. Altshuler, A. Aronov, P. Lee, *Phys. Rev. Lett.* **1980**, *44*, 1288.
[38] E. Abrahams, P. Anderson, P. Lee, T. Ramakrishnan, *Phys. Rev. B* **1981**, *24*, 6783.
[39] G. Bergmann, *Physics Reports* **1984**, *107*, 1.
[40] N. W. Preyer, M. A. Kastner, C. Y. Chen, R. J. Birgeneau, Y. Hidaka, *Phys. Rev. B* **1991**, *44*, 407.
[41] a)A. K. Nigam, A. K. Majumdar, *Phys. Rev. B* **1983**, *27*, 495; b)S. Maekawa, H. Fukuyama, *J. Phys. Soc. Jpn. 50*, 2516; c) A. Frano, E. Schierle, M. W. Haverkort, Y. Lu, M. Wu, S. Blanco-Canosa, U. Nwankwo, A. V. Boris, P. Wochner, G. Cristiani, H. U. Habermeier, G. Logvenov, V. Hinkov, E. Benckiser, E. Weschke, B. Keimer, *Phys. Rev. Lett.* **2013**, *111*, 106804.
[42] M. Sup Choi, G.-H. Lee, Y.-J. Yu, D.-Y. Lee, S. Hwan Lee, P. Kim, J. Hone, W. Jong Yoo, *Nat. Commun.* **2013**, *4*, 1624.